Front. Struct. Civ. Eng. 2023, 17(7): 1011–1020
https://doi.org/10.1007/s11709-023-0956-z

RESEARCH ARTICLE

# Numerical and experimental analyses of methane leakage in shield tunnel

**Jie HE[a,b,c], Hehua ZHU[a,b,c], Xiangyang WEI[a,b,c], Rui JIN[a,b,c], Yaji JIAO[a,b,c], Mei YIN[a,b,c,d*]**

[a] *College of Civil Engineering, Tongji University, Shanghai 200092, China*
[b] *State Key Laboratory for Disaster Reduction in Civil Engineering, Tongji University, Shanghai 200092, China*
[c] *Key Laboratory of Geotechnical and Underground Engineering of Ministry of Education, Tongji University, Shanghai 200092, China*
[d] *Department of Civil and Environmental Engineering, Brunel University, London UB8 3PH, UK*
[*] *Corresponding author. E-mail: mei.yin@brunel.ac.uk*



**ABSTRACT** Tunnels constructed in gas-bearing strata are affected by the potential leakage of harmful gases, such as methane gas. Based on the basic principles of computational fluid dynamics, a numerical analysis was performed to simulate the ventilation and diffusion of harmful gases in a shield tunnel, and the effect of ventilation airflow speed on the diffusion of harmful gases was evaluated. As the airflow speed increased from 1.8 to 5.4 m/s, the methane emission was diluted, and the methane accumulation was only observed in the area near the methane leakage channels. The influence of increased ventilation airflow velocity was dominant for the ventilation modes with two and four fans. In addition, laboratory tests on methane leakage through segment joints were performed. The results show that the leakage process can be divided into "rapid leakage" and "slight leakage", depending on the leakage pressure and the state of joint deformation. Based on the numerical and experimental analysis results, a relationship between the safety level and the joint deformation is established, which can be used as guidelines for maintaining utility tunnels.

**KEYWORDS** shield tunnel, harmful gas leakage, numerical analysis, laboratory test

## 1 Introduction

When tunnels are constructed in gas-bearing strata, they are affected by the potential leakage of harmful gases, such as methane and sulfur dioxide. High levels of these harmful gases can displace oxygen and nitrogen, potentially causing health problems. In addition, methane is highly flammable and explodes at concentrations ranging between 5% and 15%. Many disasters induced by methane leakage have been reported [1–8]. A sewage tunnel was built in Shanghai near the Yangtze River, and the release of shallow-buried methane caused a large displacement of the strata, resulting in the fracture of the tunnel [9,10]. During the geological investigation of Hangzhou Metro Line 1 project, it was observed that high-pressure methane was buried 15–30 m below the ground level, and gas eruption and combustion occurred several times during the shield tunnel construction [11,12]. A methane explosion occurred inside the excavation chamber of an Earth pressure balance (EPB)-tunnel boring machine (TBM) in Silivri–Istanbul, Europe, resulting in varying degrees of injury of 10 people [6]. Therefore, it is necessary to investigate the ventilation and diffusion of harmful gases in shield tunnels built in gas-bearing strata [13–16].

Forced ventilation is the most effective and common measure against harmful gas leakage in tunnels. Parra et al. [17] established a computational fluid dynamics (CFD) model to perform numerical analyses of different ventilation systems in deep mines. The methane diffusion characteristics obtained from analyses were compared with different criteria. Sasmito et al. [18] analyzed the methane distribution in a coal mine roadway using numerical simulations, providing a reference for optimizing ventilation systems to reduce gas concentration. Other scholars have investigated the

*Article history: Received Jun 29, 2022; Accepted Dec 7, 2022*

ventilation systems of ordinary tunnels, and their methods have reference significance for analyzing gas tunnel ventilation. Camelli et al. [19] simulated the airflow in subway tunnels and stations. They used spatial complexity and temporal stability to quantify the airflow dynamics. Amouzandeh et al. [20] developed a three-dimensional CFD model to simulate fires in railway tunnels under various ventilation conditions. Wei et al. [21] evaluated the diffusion of harmful gases during the construction of rock tunnels using numerical simulations. They observed that the vortices near the tunnel face significantly influenced the diffusion of harmful gases. Kang et al. [22] used CFD software to simulate a tunnel ventilation system and assessed the gas concentration near the tunnel face. Kurnia et al. [23] simulated the methane dispersion inside a mine tunnel and found that the methane concentration could be reduced below the safety level through appropriate ventilation. Fang et al. [24] investigated the airflow behavior and hazardous gas dispersion in the ventilation system of a twin-tunnel structure. The results showed that local jet fans could effectively eliminate the "dead zone" ahead of the cross-aisle. Fang et al. [25] investigated the airflow near the work face by constructing CFD models and predicted the gas distribution in a gas tunnel structure. Li et al. [26] developed a multicomponent Lattice Boltzmann Method (LBM)-Large Eddy Simulation (LES) model to simulate methane flow in tunnels and conducted a reduced-scale tracer gas experiment to validate the numerical analysis.

Most of these studies focused on the diffusion of harmful gases induced during mining or tunnel construction; however, few studies on the leakage and diffusion of harmful gases through tunnel joints during tunnel operation have been conducted. In this study, a steady-state numerical analysis was performed to simulate gas leakage through tunnel joints and the diffusion of harmful gases in a shield tunnel in operation. In addition, laboratory tests on methane leakage through segment joints were performed to validate the numerical model. On the basis of numerical and experimental analyses, safety levels based on the joint deformations of the entire tunnel segment were established.

## 2 Methodology

### 2.1 Project description

This study was based on a utility tunnel constructed in China. Geological investigation indicated that shallow-buried methane existed under the Yangtze River bed. The most frequent leakage channels of harmful gases in shield tunnels are the segment joints [27,28]. If the gasketed segment joints malfunction, high-pressure methane will leak through the tunnel joints and, thus, affect the safety of the entire tunnel. The outer diameter of the tunnel was 11.6 m, and its total length was approximately 5468 m. The deepest point of the tunnel was approximately 80 m below the water level (Fig. 1).

The cross-section of the tunnel was divided into several chambers (Fig. 2), and most utility lines (for example, high-voltage electricity lines) were installed in the upper chamber. Several ladders existed between the upper and lower chambers. The ventilation system consisted of six fans (divided into three groups) located at the top of the upper chamber (Fig. 2). Additionally, methane-monitoring sensors were installed on the tunneling lining to monitor the real-time methane concentration.

### 2.2 Mathematical formulation of gas flow in tunnel

In this study, the gases were assumed to be released from the tunnel joints and dispersed by ventilation airflow to simulate the leakage and diffusion of harmful gases through tunnel joints during the tunnel operation. The laws of conservation in physics govern the leakage and diffusion processes of harmful gases, including the conservation equations for mass, momentum, energy, and species.

1) Conservation equation for mass

$$\frac{\partial \rho}{\partial t} + \operatorname{div}(\rho \vec{v}) = 0, \tag{1}$$

where $\rho$ is the density, and $\vec{v}$ is the flow velocity.

2) Conservation equations for momentum

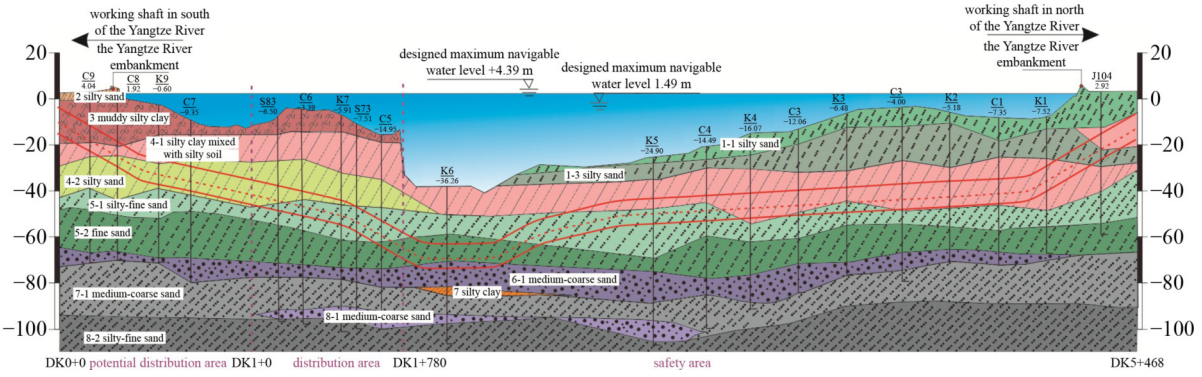


**Fig. 1** Stratigraphic layer and division of shallow gas.

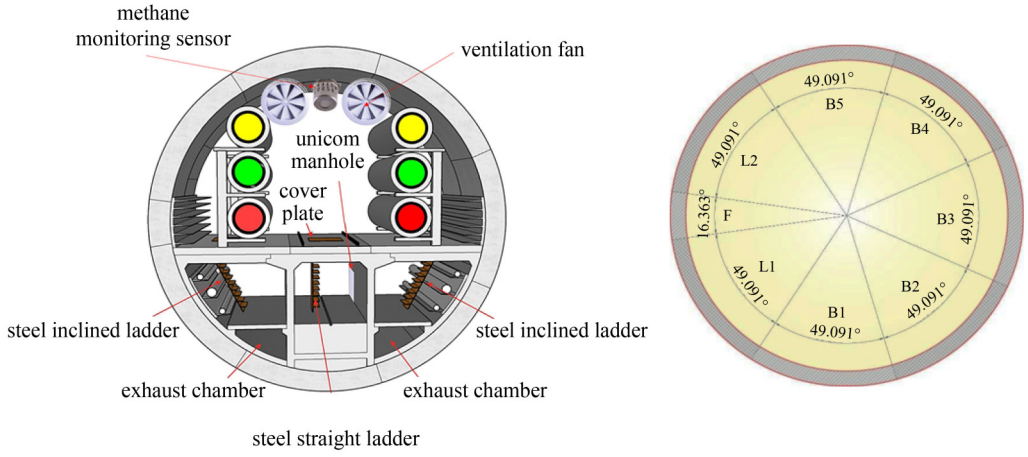


**Fig. 2** Schematic of utility tunnel.

$$\frac{\partial}{\partial t}(\rho\vec{v})+\mathrm{div}(\rho v_i\vec{v})-\mathrm{div}(\mu_e\mathrm{div}\,\vec{v})=\mathrm{div}p'+B, \quad (2)$$

where $v_i$ is a scalar of velocity vector $\vec{v}$, $\mu_e$ is the effective diffusion coefficient, $B$ is the sum of forces per unit volume of fluid elements, and $p'$ is the pressure per unit area of the fluid microelement after modification. $p'$ can be defined as

$$p'=p+\frac{2}{3}\rho k, \quad (3)$$

where $k$ is the turbulent kinetic energy. In addition, the effective diffusion coefficient, $\mu_e$, satisfies

$$\mu_e=\mu+\mu_t, \quad (4)$$

where $\mu$ is the dynamic viscosity, and $\mu_t$ is the turbulent viscosity.

The $k$–$\varepsilon$ model [16] assumes that the turbulent viscosity is related to the turbulent kinetic energy $k$ and turbulent dissipation rate $\varepsilon$ as follows:

$$\mu_t=\frac{C_\mu\rho k^2}{\varepsilon}, \quad (5)$$

where $C_\mu$ is an empirical constant. The turbulent kinetic energy, $k$, and turbulent dissipation rate, $\varepsilon$, were solved using the following partial differential equations.

$$\frac{\partial}{\partial t}(\rho k)+\mathrm{div}(\rho k\vec{v})=\mathrm{div}\left[\left(\mu+\frac{\mu_t}{\sigma_k}\right)\mathrm{div}k\right]+P_k-\rho\varepsilon, \quad (6)$$

$$\frac{\partial}{\partial t}(\rho\varepsilon)+\mathrm{div}(\rho\varepsilon\vec{v})=\mathrm{div}\left[\left(\mu+\frac{\mu_t}{\sigma_\varepsilon}\right)\mathrm{div}\varepsilon\right]+\frac{\varepsilon}{k}(C_{\varepsilon1}P_k-C_{\varepsilon2}\rho\varepsilon), \quad (7)$$

where $\sigma_k$ and $\sigma_\varepsilon$ are the Prandtl numbers corresponding to the turbulent kinetic energy $k$ and dissipation rate $\varepsilon$, respectively, $P_k$ represents the influence of viscosity and buoyancy, and $C_{\varepsilon1}$ and $C_{\varepsilon2}$ are empirical constants.

3) Conservation equation for energy

$$\frac{\partial}{\partial t}(\rho T)+\mathrm{div}(\rho\vec{v}T)=\mathrm{div}\left(\frac{k_T}{c_p}\mathrm{grad}T\right)+S_T, \quad (8)$$

where $c_p$ is the heat capacity, $k_T$ is the heat transfer coefficient of the fluid, and $S_T$ is the internal heat source.

4) Conservation equation for species

$$\frac{\partial}{\partial t}(\rho c_s)+\mathrm{div}(\rho\vec{v}c_s)=\mathrm{div}(D_s\mathrm{grad}(\rho c_s))+S_s, \quad (9)$$

where $c_s$ is the volume concentration of component $s$, $\rho c_s$ is the mass concentration of the component, and $D_s$ is the mass of the component produced during the chemical reaction per unit volume within a unit of time in the system, called productivity.

Ventilation air comprises three species: oxygen, nitrogen, and methane. The specified mole fraction of methane in this study was 0.85, according to the geological investigation report. The interaction between the species obeys the incompressible ideal gas law proposed by Kurnia et al. [23].

### 2.3 Mathematical formulation of gas flow through segment joints

Ren et al. [29] derived the governing equation of compressible gas flow through the interface of two static rough surfaces (Fig. 3), which can be expressed as

$$\frac{\partial}{\partial x}\left(\phi_x\frac{\overline{p}h^3}{12\mu}\frac{\partial\overline{p}}{\partial x}\right)+\frac{\partial}{\partial y}\left(\phi_y\frac{\overline{p}h^3}{12\mu}\frac{\partial\overline{p}}{\partial y}\right)=0, \quad (10)$$

where $\overline{p}$ is the average fluid pressure, $h$ is the average thickness of the liquid film, $\mu$ is the viscosity of the fluid, and $\phi_x$ and $\phi_y$ are the pressure flow factors in the $x$- and $y$-direction, respectively. The pressure flow factors represent the ratio of the average flow rate of the rough surface to that of the smooth surface with the same average thickness of the liquid film.

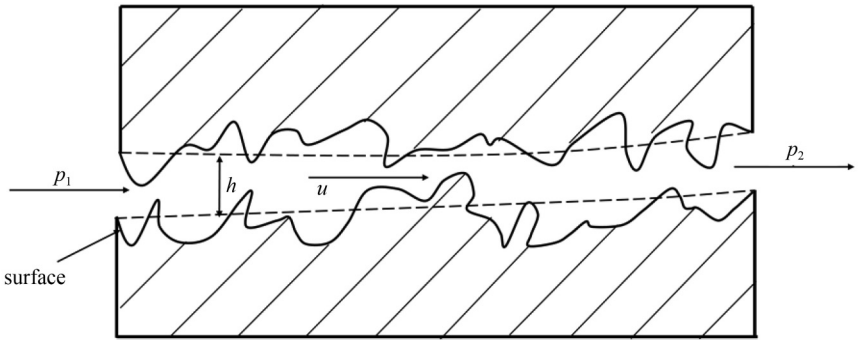


**Fig. 3** Geometric characteristics of rough surfaces.

The average leakage rate of gases flowing through the leakage channel between two rough surfaces can be expressed by

$$q_{\mathrm{m}} = \phi_x \frac{lh^3}{24\mu R_{\mathrm{g}} T} \frac{p_1^2 - p_2^2}{b}, \tag{11}$$

where $l$ is the length of the interface, $R_{\mathrm{g}}$ is the gas constant, $b$ is the width of the interface (path length of the gas leakage channel), and $p_1$ and $p_2$ are the gas pressures at the entrance and exit of the interface, respectively. According to Patir and Cheng [30], the following pressure flow factors $\phi_x$ can be derived:

$$\begin{aligned} \phi_x &= 1 - D\mathrm{e}^{-R(h/\sigma)}, \quad \gamma \leqslant 1, \\ \phi_x &= 1 + D\mathrm{e}^{-R}, \quad \gamma > 1, \end{aligned} \tag{12}$$

where $\gamma$ is the eigenvalue characterizing the roughness texture direction, $D$ and $R$ are the parameters related to $\gamma$, and the root mean square of the combined root-mean-square roughness, $\sigma$, can be obtained using experimental instruments.

The parameters for the gas flow in the segment joints are listed in Table 1. These parameters were derived according to Ren et al. [29].

**Table 1** Parameters used in leakage rate computations

| item | $\sigma$ (μm) | $D$ | $R$ | $T$ (K) | $\mu$ (Pa·s) | $R_{\mathrm{g}}$ (J·kg$^{-1}$·K$^{-1}$) |
|---|---|---|---|---|---|---|
| segment joints | 0.30 | 1 | 0.54 | 293.15 | $1.81 \times 10^{-5}$ | 286.7 |

## 2.4 Establishment of model

Half of the upper-tunnel chamber was simulated in this study owing to the symmetry of the tunnel (Fig. 4). This part of the tunnel contained three high-voltage electricity lines. The outer diameter of each line was 1.4 m, the distance between the axes of the adjacent lines was 1.5 m, and the center of the lowest line on the tunnel section was 1 m above the ground and 2.7 m from the symmetry plane (Fig. 4(a)). Because the electricity lines were assumed to be completely airtight, they were ignored in the numerical simulations. As segment joints are the most frequent gas leakage channel [27,28], a set of circumferential and longitudinal joints was set as the inlet of the harmful gases (Figs. 4(b) and 4(c)). The width of the joints was set to 13 mm. The total lengths of the tunnel model of the computational mesh for the two and three channels were 33 and 44 m, respectively. Six ventilation fans were installed in the tunnel, which operated in four modes. The ventilation airflow velocities were 0, 1.8, 3.6, and 5.4 m/s for the operations of zero, two, four, and six fans, respectively. In this study, ICEM was used to establish the CFD model and mesh. Next, the CFD model was imported into FLUENT software. The boundary conditions of this model are as follows. (i) The pressure at the entrance of the gas leakage channel was set to 0.4 MPa. (ii) At the inlet, the airflow velocities were 0, 1.8, 3.6, and 5.4 m/s based on the different ventilation modes. (iii) At the circumferential joints of the segment

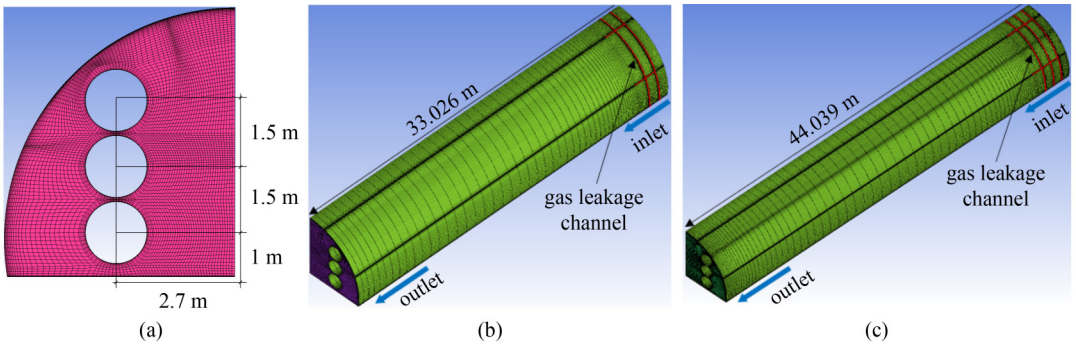


**Fig. 4** Schematic and computational domain of shield tunnel: (a) cross-section; (b) computational mesh of two channels; (c) computational mesh of three channels.

lining near the inlet, the gases were released under pressure of 0.4 MPa along the circumferential and longitudinal joints. (iv) At the outlet, the pressure was set to the standard atmospheric pressure.

## 3 Numerical results and discussion

The computed leakage rates were defined as the mass leakage rates through a leakage channel of 1 m in length. A comparison between the numerical analysis and laboratory test is shown in Fig. 5. The computational results were consistent with the test results, particularly at relatively low leakage pressures. When the leakage pressure exceeded 0.6 MPa, the computed leakage rates deviated from the test results, but their variation trends were still similar.

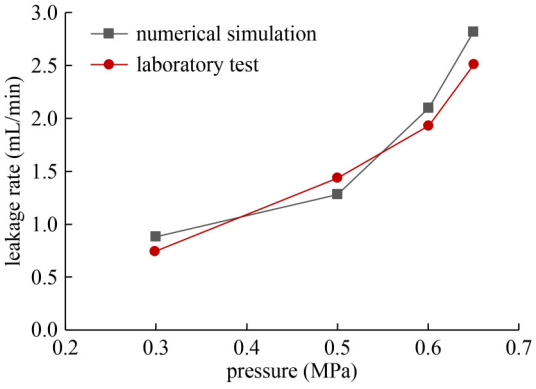


**Fig. 5** Comparison between numerical simulation and laboratory test values of leakage rate.

Figure 6 shows the distributions of methane concentration for different ventilation modes in the tunnel with two leakage channels. The methane was mainly distributed near the upper area of the tunnel segment, which is consistent with the fact that the density of methane is lower than that of air. In addition, when the ventilation airflow velocity in the tunnel was 1.8 m/s, the methane gas accumulated in the area near the tunnel segment owing to buoyancy. As the airflow velocity increased to 5.4 m/s, the methane emission became diluted, and methane accumulation was only observed near the methane leakage channel. This indicates that ventilation can sufficiently dilute methane emissions. However, when the ventilation airflow velocity increased from 1.8 to 5.4 m/s, the maximum methane concentration decreased from 74.5% to 73.5%. This indicates that the influence of ventilation on the maximum methane concentration is limited because the maximum concentration occurs near the outlet of the leakage channel, which is very close to the methane source.

Figure 7 shows the distribution of methane concentration in tunnel with three leakage channels in different ventilation modes. The methane concentration distribution shown in Fig. 7 is similar to that in Fig. 6. The methane accumulated at the top of the tunnel owing to buoyancy. With three leakage channels, most of the methane emissions were diluted by the ventilation system. Some of the methane accumulated in the area

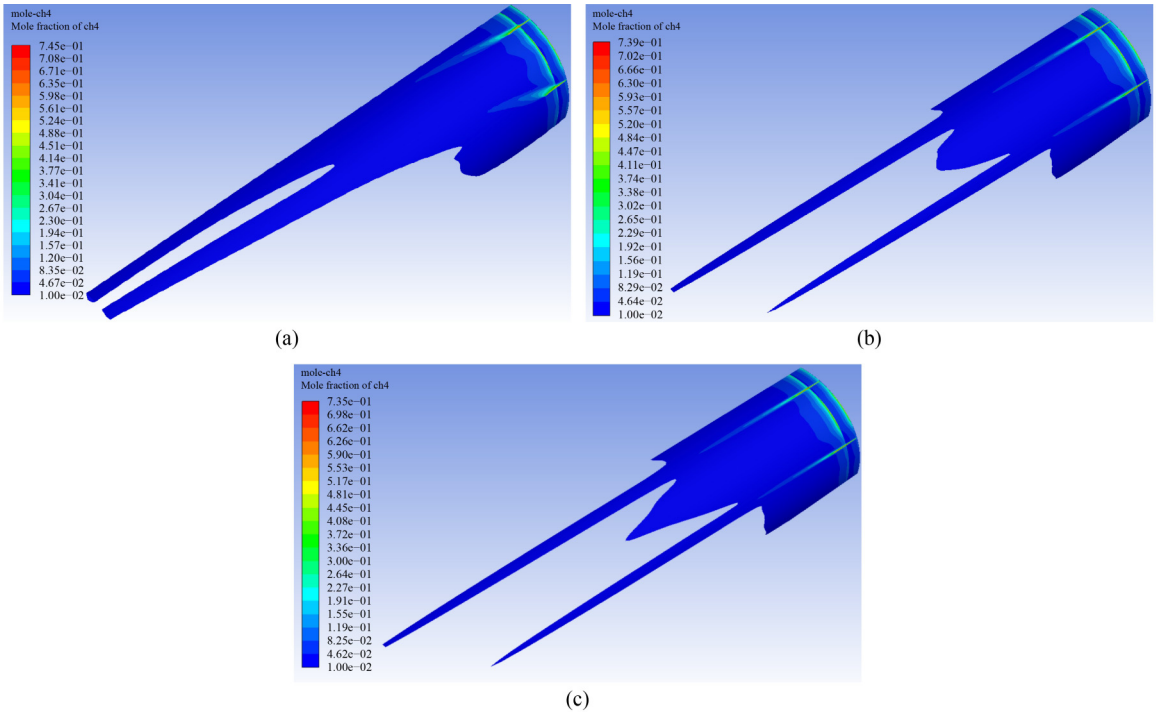


**Fig. 6** Distribution of methane concentration in tunnel with two leakage channels: (a) 1.8 m/s; (b) 3.6 m/s; (c) 5.4 m/s.

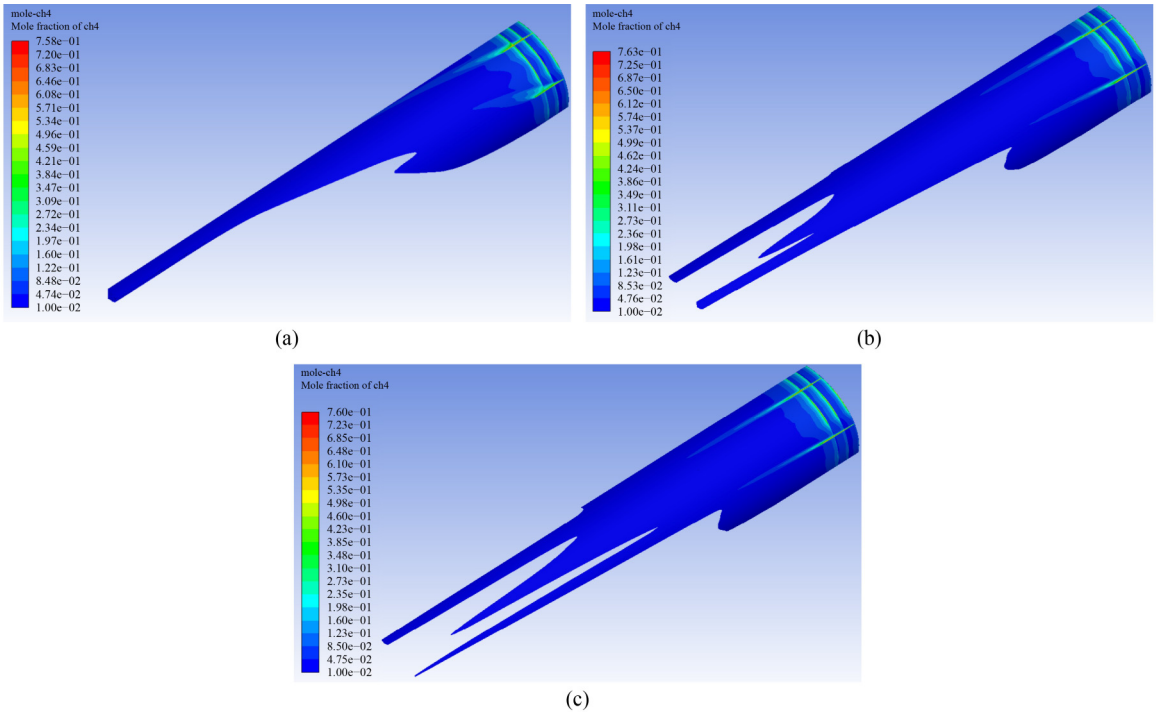


**Fig. 7** Distribution of methane concentration in tunnel with three leakage channels: (a) 1.8 m/s; (b) 3.6 m/s; (c) 5.4 m/s.

near the segment joints. However, the distribution area with methane concentration higher than 1% was significantly larger than that in the case of two leakage channels. This trend demonstrates that the leakage rate is dominant in the accumulation area of methane. Because of the high-voltage electricity lines installed in the tunnel, it is necessary to dilute the methane emission to a safe and acceptable level. When significant methane accumulation is observed, the tunnel must be closed immediately.

According to the Chinese standard, Technical standard for supervision and alarm system engineering of urban utility tunnel, the methane concentration limit for personnel work and safe operation of electrical equipment is 0.25%*v*/*v*. Accordingly, the distribution area where the methane concentration exceeded 0.25%*v*/*v* was plotted (Fig. 8). When two fans were in operation, the ventilation airflow velocity was approximately 1.8 m/s, according to the field monitoring data. The leakage rates of methane through the segment joints were set to $Q$ = 230, 390, and 550 mL·min$^{-1}$·m$^{-1}$ (Fig. 8). Methane accumulated in the area near the inner wall of the tunnel, and the thickness of the accumulation area at the top of the chamber was the largest. In addition, the envelope thickness of the accumulation area increased with an increasing leakage rate, and the largest thickness was approximately 1.5 m at the top of the chamber. In a ventilation mode of four fans ($v$ = 3.6 m/s), the calculated distributions of methane with a concentration exceeding 0.25% were plotted (Figs. 8(d)–8(f)). The distribution pattern of methane concentration is similar to the case of two fans ($v$ = 1.8 m/s). However, the thickness of the accumulation area decreased at the top of the tunnel compared to the first ventilation mode. Figures 8(g)–8(i) shows the distribution of methane with a concentration exceeding 0.25% in a ventilation mode of six fans ($v$ = 5.4 m/s). The ventilation effect of the six fans is similar to that of the four fans. This indicates a negligible effect of adding ventilation fans on the dilution in the accumulation area at the top of the tunnel.

According to Chinese standards, for example, Technical standard for supervision and alarm system engineering of urban utility tunnel, Technical standard for operation, maintenance and safety management of urban utility tunnel, and Code for design of electrical installations in explosive atmospheres, the safety of tunnels can be divided into five levels based on the methane concentration (volume fraction), as listed in Table 2. For example, if the methane concentration is lower than 0.25%*v*/*v*, the tunnel is suitable for onsite work and safe for the operation of electrical utilities. However, there is a risk of an explosion if the methane concentration exceeds 2%*v*/*v*. Adequate safety measures should be applied to ensure the methane concentration decreases below the explosive limit.

The methane concentration at the location of the methane-monitoring sensor (0.25 m below the top of the tunnel lining) can be determined from the steady-state numerical analysis. The relationship between the methane concentration and the leakage rate is shown in Fig. 9. When the two fans were operating, the methane

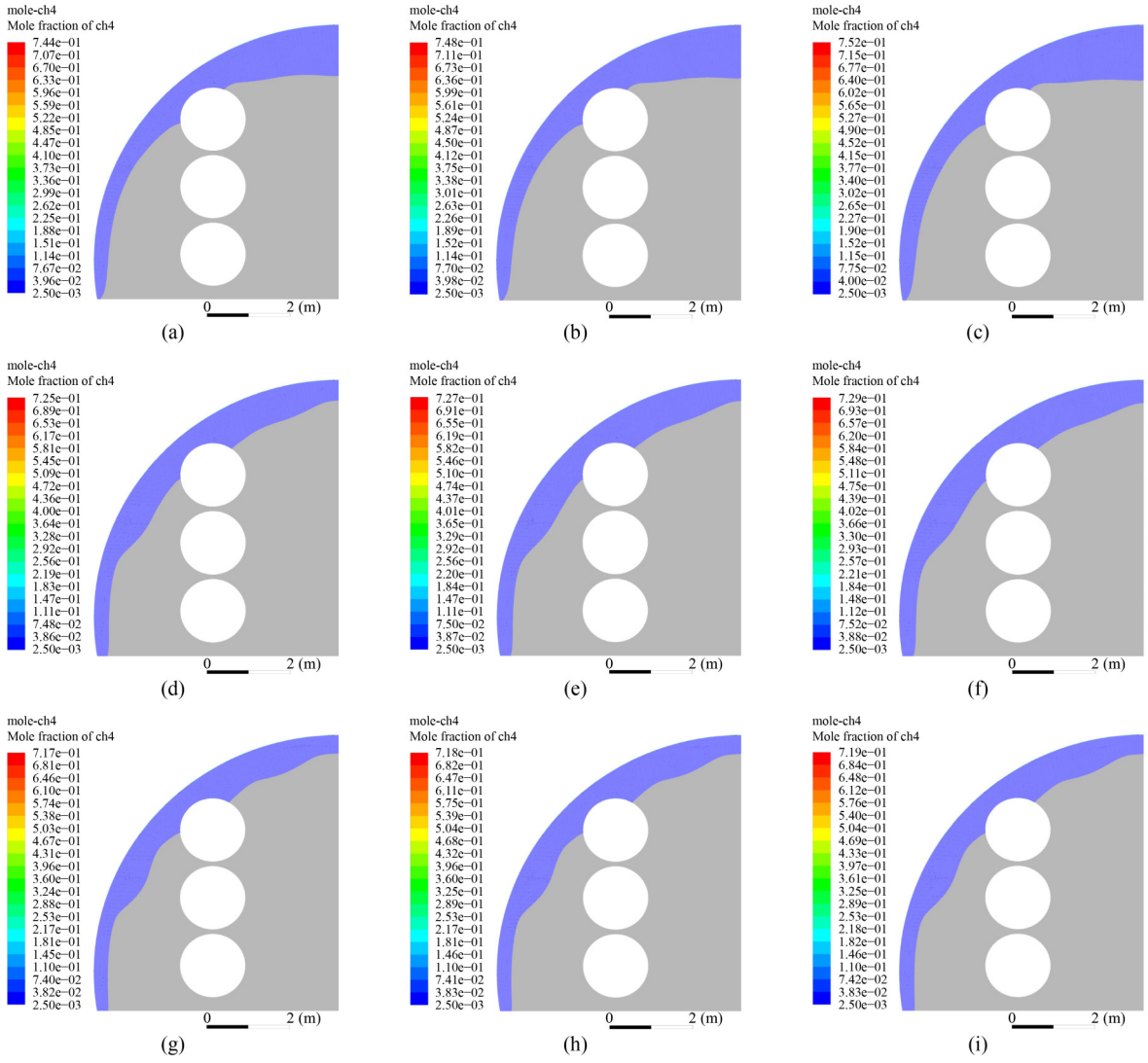


**Fig. 8** Distribution areas of methane concentration exceeding 0.25%*v*/*v* for different leakage rates ($Q$) and airflow velocities ($v$): (a) $Q$ = 230 mL·min$^{-1}$·m$^{-1}$ & $v$ = 1.8 m/s; (b) $Q$ = 390 mL·min$^{-1}$·m$^{-1}$ & $v$ = 1.8 m/s ; (c) $Q$ = 550 mL·min$^{-1}$·m$^{-1}$ & $v$ = 1.8 m/s; (d) $Q$ = 230 mL·min$^{-1}$·m$^{-1}$ & $v$ = 3.6 m/s; (e) $Q$ = 390 mL·min$^{-1}$·m$^{-1}$ & $v$ = 3.6 m/s; (f) $Q$ = 550 mL·min$^{-1}$·m$^{-1}$ & $v$ = 3.6 m/s ; (g) $Q$ = 230 mL·min$^{-1}$·m$^{-1}$ & $v$ = 5.4 m/s; (h) $Q$ = 390 mL·min$^{-1}$·m$^{-1}$ & $v$ = 5.4 m/s; (i) $Q$ = 550 mL·min$^{-1}$·m$^{-1}$ & $v$ = 5.4 m/s.

**Table 2** Safety levels based on methane concentration

| safety level | methane concentration (*v*/*v*) | remark |
|---|---|---|
| 1 | < 0.25% | The environment is suitable for onsite work and safe for the operation of electrical utilities. |
| 2 | 0.25%–0.5% | Onsite workers should adopt protective measures, and the operation of electric utilities is still safe. |
| 3 | 0.5%–1% | Onsite workers should adopt protective measures, but there are risks to the operation of electrical utilities. |
| 4 | 1%–2% | The methane concentration-monitoring alarm will be triggered. |
| 5 | > 2% | There are risks of explosion. |

concentration sharply increased with the leakage rate. When the leakage rate reached approximately 220 mL·min$^{-1}$·m$^{-1}$, the methane concentration increased to 2%, which is the limit of safety level 5. Thus, the two fans could not efficiently dilute methane in this case. However, when four and six fans were activated, the methane concentration decreased to 0.4% and 0.3%, respectively, causing the tunnel to fall into safety level 2. This indicates that the influence of increasing the ventilation airflow velocity is more pronounced for the ventilation modes with two and four fans than that with six fans.

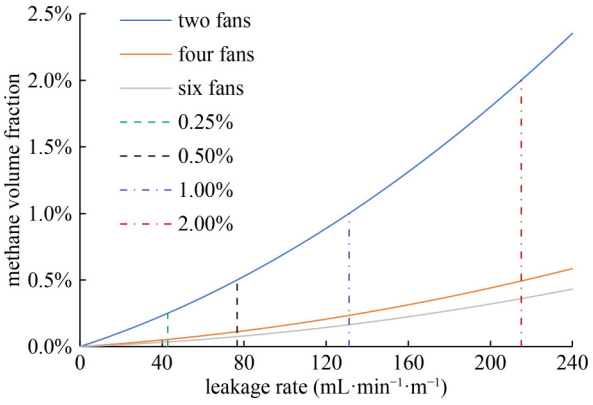


**Fig. 9** Variation in methane concentration with leakage rate under ventilation conditions of different numbers of fans.

## 4 Experimental analysis of methane leakage through segment joints

Figure 9 shows the relationship between the methane concentration and the leakage rate. However, it is challenging to directly measure the methane leakage rate through tunnel joints. A more practical method is to determine the potential relationship between the safety level and the joint deformation, that is, the joint opening ($A$) and joint dislocation ($S$). Hence, gas leakage tests were performed (Fig. 10). The test apparatus consisted of the following: (a) a segment joint model, including sealing gaskets and concrete plates with gasket grooves; (b) a reaction frame and load controller to control the joint deformations; (c) a pump to drive high-pressure air into the segment joint; (d) flowmeters to measure the leakage rate; (e) temperature sensors; and (f) pressure sensors. During the gas leakage tests, pressurized air was applied to the gasket joint using the air pump after the segment joint was subjected to loads and deformations. The airflow rate was measured using the flowmeters. Hence, the relationship between the methane leakage rate and the joint deformation was determined.

As mentioned above, tests were conducted on the performance of the gas leakage through segment joints. The joint deformation state, that is, the joint opening ($A$), joint dislocation ($S$), and leakage pressure, were the main factors evaluated in the tests. The test setup parameters are listed in Table 3.

The variation in the leakage rate with leakage pressure during the entire test process is shown in Fig. 11. Most of the tests initially indicated a minimal increase in the leakage rate with increasing leakage pressure, followed by a breakpoint. Hence, two types of leakage, "rapid leakage" and "slight leakage", were observed. These two processes can be differentiated based on the relationship between the leakage rate and the pressure (Fig. 11).

Both leakage types significantly differed in magnitude, depending on the leakage pressure and the joint deformation state (joint opening $A$ and joint dislocation $S$). As the pressure increased, the leakage rate increased from 0.1 to 1.0 mL/min, and the process is called "slight leakage." The leakage rate significantly changed when it exceeded 1.0 mL/min, and this process is called "rapid leakage." For large joint openings (openings exceeding 8 mm in width), the gas sealing behavior finally failed, and "rapid leakage" occurred when the leakage pressure was sufficiently high. However, at low leakage pressures, the sealing gaskets exhibited good behavior, and only a "slight leakage" occurred. For small joint openings, the leakage rate was lower than 1.0 mL/min when the leakage pressure was lower than 2.3 MPa.

By combining the results in Table 2 and Figs. 9 and 11, with the geometry of the tunnel segments, the safety levels based on the joint deformations of the entire tunnel segment were identified (Table 4). All the numerical analyses discussed in the previous section were based on steady-state analysis. The safety level changed after the tunnel underwent long-term deformations (Table 4). For example, if the joint opening reaches 36 mm and the joint dislocation reaches 24 mm, the tunnel will be at a dangerous safety level with a risk of explosion. Hence, the results presented in Table 4 can be used as guidelines for maintaining shield tunnels passing through gas-bearing strata.

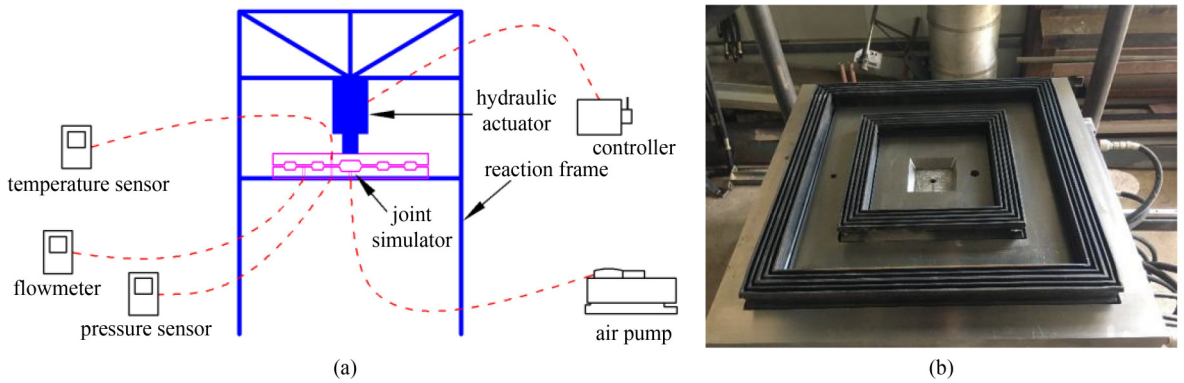


**Fig. 10** Schematic of gas leakage test setup: (a) test setup; (b) sealing gasket.

**Table 3** Test setup parameters

| test set | joint opening (mm) | joint dislocation (mm) |
|---|---|---|
| test 2 | 4, 6, 8, 10, 13, 15 | 0, 10 |

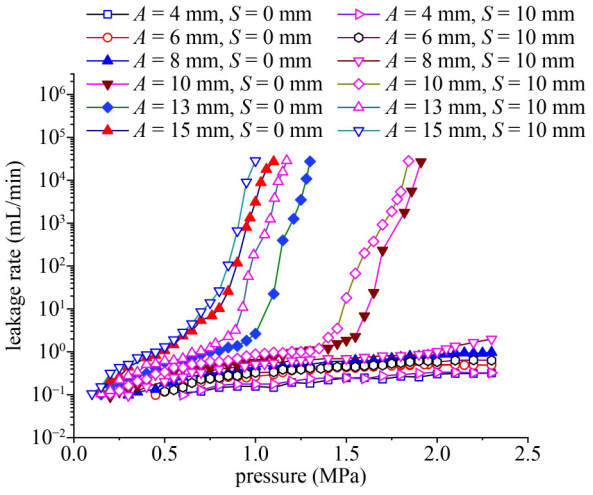


**Fig. 11** Test results of air leakage induced by joint deformations.

**Table 4** Joint openings and joint dislocations at different safety levels

| safety level | methane concentration (*v*/*v*) | joint opening | joint dislocation |
|---|---|---|---|
| 1 | < 0.25% | $A \leqslant 18$ mm | 0 mm $\leqslant S <$ 8 mm |
| 2 | 0.25%–0.5% | 18 mm $< A \leqslant$ 24 mm | 8 mm $\leqslant S <$ 12 mm |
| 3 | 0.5%–1% | 24 mm $< A \leqslant$ 30 mm | 12 mm $\leqslant S <$ 16 mm |
| 4 | 1%–2% | 30 mm $< A \leqslant$ 36 mm | 16 mm $\leqslant S <$ 24 mm |
| 5 | > 2% | $A >$ 36 mm | $S \geqslant$ 24 mm |

## 5 Conclusions

When tunnels are constructed in gas-bearing strata, they are affected by the potential leakage of harmful gases, such as methane gas. The aim of this study was to investigate the effect of methane leakage on the safety level of shield tunnels in operation. Combined numerical and experimental analyses were performed on the leakage, ventilation, and diffusion of harmful gases in a shield tunnel. Based on the findings, the main conclusions are as follows.

(1) Methane was mainly distributed near the upper area of the tunnel segment. This is consistent with the fact that the density of methane is lower than that of air.

(2) As the airflow velocity increased from 1.8 to 5.4 m/s, the methane emission was diluted, and methane accumulation was only observed near the methane leakage channels.

(3) The numerical analysis showed that two fans could not efficiently dilute the methane. However, when four and six fans were activated, the methane concentration decreased to 0.4% and 0.3%, respectively. Hence, the increase in the ventilation airflow velocity was more dominant for the ventilation modes of two and four fans than for that of 6 fans.

(4) Laboratory tests were performed on methane leakage through segment joints to validate the numerical model. The results showed a minimal initial increase in the leakage rate with increasing leakage pressure, followed by a breakpoint. Hence, this process can be divided into “rapid leakage” and “slight leakage” stages, depending on the leakage pressure and the joint deformation state.

(5) Based on the numerical and experimental analysis results, the relationship between the safety level and the joint deformation (the joint opening and joint dislocation) was established. This relationship can be used as a convenient guideline for maintaining utility tunnels.

However, limitations existed in this study, including the following. (i) The numerical analysis results require improved validation. (ii) Some models in this study are too ideal, so the actual situation of gas leakage in tunnels should be considered. (iii) Parametric studies to extensively investigate the ventilation and diffusion of harmful gases in shield tunnels should be conducted.

**Acknowledgements** We thank Mr Rui Jin (Tongji University) and Mr Yaji Jiao (Tongji University) for assistance in the research. This study was funded by the China Postdoctoral Science Foundation (No. 2019M651580) and the Research Project of the Chinese National Major Scientific Instrument and Equipment Development (No. 41827807). The authors gratefully acknowledge this support.



**Conflict of Interest** The authors declare that they have no conflict of interest.

## References

1. Pearson F. How to avoid an explosive situation. Tunnels & Tunnelling International, 1991, 23(9): 27−29
2. Proctor R J. The San Fernando tunnel explosion, California. Engineering Geology, 2002, 67(1–2): 1–3

3. Vlasov S N, Makovsky L V, Merkin V E. Accidents in Transportation and Subway Tunnels: Construction to Operation. Moscow: Elex-KM Publishers, 2001
4. Pearson C F C, Edwards J S, Durucan S. Methane occurrences in the Carsington Aqueduct tunnel project—A case study. In: Proceedings of the Rapid Excavation and Tunneling Conference. Los Angeles: 1989: 11–14
5. Jaffe W, Lockyer R, Howcroft A. The Abbeystead explosion disaster. Annals of Burns and Fire Disasters, 1997, 10(3): 1−4
6. Copur H, Cinar M, Okten G, Bilgin N. A case study on the methane explosion in the excavation chamber of an EPB-TBM and lessons learnt including some recent accidents. Tunnelling and Underground Space Technology, 2012, 27(1): 159−167
7. Kang X B, Xu M, Luo S, Xia Q. Study on formation mechanism of gas tunnel in non-coal strata. Natural Hazards, 2013, 66(2): 291−301
8. Morsali M, Rezaei M. Assessment of $H_2S$ emission hazards into tunnels: The Nosoud tunnel case study from Iran. Environmental Earth Sciences, 2017, 76(5): 227
9. Tang Y Q, Ye W M, Zhang Q H. Marsh gas in soft stratum at the estuary of the Yangtze river and safety measures of construction of the tunnel. Journal of Tongji University (Natural Science), 1996, 24(4): 465–470 (in Chinese)
10. Tang Y Q, Liu B Y, Zhad S K, Huang Y. Research on influence of high-pressure marsh gas on sandy silt engineering. Journal of Tongji University (Natural Science), 2004, 32: 1316–1319 (in Chinese)
11. Guo A, Shen L, Zhang J, Qin J, Huang X, Wang Y. Analysis of influence mode of shallow gas on construction of Hangzhou Metro. Journal of Railway Engineering Society, 2010, 27(9): 78−81
12. Guo A G, Kong L W, Shen L C, Zhang J R, Wang Y, Qin J S, Huang X F. Study of disaster countermeasures of shallow gas in metro construction. Rock and Soil Mechanics, 2013, 34(3): 769−775 (in Chinese)
13. Du J K. Analysis on the leaking process of toxic gases from chemical accidents and determination of the risky area. China Safety Science Journal, 2002, 12(6): 55−59
14. Luo Ai M, Wei L J. Numerical method of safety distance for poisonous dense gaseous leakage. China Safety Science Journal, 2005, 15(8): 98−100
15. Li P, Ding Y F, Weng P F. Study on leakage and dispersion of dangerous materials in highway tunnel. China Safety Science Journal, 2004, 14(10): 5
16. Wang D D, Mao L, Li J F. On the application of FLUENT to the dispersion of poisonous gases in highway tunnels. Journal of Safety and Environment, 2008, 8(2): 140−143
17. Parra M T, Villafruela J M, Castro F, Mendez C. Numerical and experimental analysis of different ventilation systems in deep mines. Building and Environment, 2006, 41(2): 87−93
18. Sasmito A P, Birgersson E, Ly H C, Mujumdar A S. Some approaches to improve ventilation system in underground coal mines environment—A computational fluid dynamic study. Tunnelling and Underground Space Technology, 2013, 34: 82−95
19. Camelli F E, Byrne G, Löhner R. Modeling subway air flow using CFD. Tunnelling and Underground Space Technology, 2014, 43: 20−31
20. Amouzandeh A, Zeiml M, Lackner R. Real-scale CFD simulations of fire in single-and double-track railway tunnels of arched and rectangular shape under different ventilation conditions. Engineering Structures, 2014, 77: 193−206
21. Wei N, Li L, Wang C Y. Analysis of harmful gases concentration variation in tunneling ventilation. Journal of China Three Gorges University, 2006, 28(4): 324−327
22. Kang X B, Ding R, Xu M, Zhao S J. Numerical simulation for the ventilation in the construction of high gas tunnel. Journal of Chengdu University of Technology (Science & Technology Edition), 2012, 39(03): 311−316
23. Kurnia J C, Sasmito A P, Mujumdar A S. CFD simulation of methane dispersion and innovative methane management in underground mining faces. Applied Mathematical Modelling, 2014, 38(14): 3467−3484
24. Fang Y, Fan J, Kenneally B, Mooney M. Air flow behavior and gas dispersion in the recirculation ventilation system of a twin-tunnel construction. Tunnelling and Underground Space Technology, 2016, 58: 30−39
25. Fang Y, Yao Z, Lei S. Air flow and gas dispersion in the forced ventilation of a road tunnel during construction. Underground Space, 2019, 4(2): 168−179
26. Li C, Zhao Y, Ai D, Wang Q, Peng Z, Li Y. Multi-component LBM-LES model of the air and methane flow in tunnels and its validation. Physica A, 2020, 553: 124279
27. Wu H N, Huang R Q, Sun W J, Shen S L, Xu Y S, Liu Y B, Du S J. Leaking behavior of shield tunnels under the Huangpu River of Shanghai with induced hazards. Natural Hazards, 2014, 70(2): 1115−1132
28. Wu J, Liu Z, Yuan S, Cai J, Hu X. Source term estimation of natural gas leakage in utility tunnel by combining CFD and Bayesian inference method. Journal of Loss Prevention in the Process Industries, 2020, 68: 104328
29. Ren X, Wu C, Zhou P. Gas sealing performance study of rough surface. Journal of Mechanical Engineering, 2010, 46(16): 176−181
30. Patir N, Cheng H S. An average flow model for determining effects of three-dimensional roughness on partial hydrodynamic lubrication. Journal of Tribology, 1978, 100(1): 12−17